Analyst

PAPER

View Article Online
View Journal | View Issue

Cite this: *Analyst*, 2014, **139**, 5800

Development of a simple bioelectrode for the electrochemical detection of hydrogen peroxide using *Pichia pastoris* catalase immobilized on gold nanoparticle nanotubes and polythiophene hybrid

Seetharamaiah Nandini,[ac] Seetharamaiah Nalini,[ac] Jakkid Sanetuntikul,[b] Sangaraju Shanmugam,[b] Pathappa Niranjana,*[c] Jose Savio Melo*[d] and Gurukar Shivappa Suresh*[a]

In this paper, a simple and innovative electrochemical hydrogen peroxide biosensor has been proposed using catalase (CAT_{pp}) derived from *Pichia pastoris* as bioelectrocatalyst. The model biocomponent was immobilized on gold nanoparticle nanotubes (AuNPNTs) and polythiophene composite using 1-ethyl-3-(3-dimethylaminopropyl)-carbodiimide and *N*-hydroxysuccinimide (EDC–NHS) coupling reagent. In this present work, we have successfully synthesized gold nanoparticles (AuNPs) by ultrasonic irradiation. The tubular gold nanostructures containing coalesced AuNPs were obtained by sacrificial template synthesis. The assembly of AuNPNTs onto the graphite (Gr) electrode was achieved *via* S–Au chemisorption. The latter was pre-coated with electropolymerized thiophene (PTh) to enable S groups to bind AuNPNTs. The combination of AuNPNTs–PTh, *i.e.*, an inorganic–organic hybrid, provides a stable enzyme immobilization platform. The physical morphology of the fabricated biosensor Gr/PTh/AuNPNTs/EDC–NHS/CAT_{pp} was investigated using scanning electron microscopy and energy-dispersive microscopy. The analytical performance of the bioelectrode was examined using cyclic voltammetry, differential pulse voltammetry and chronoamperometry. Operational parameters such as working potential, pH, and thermal stability of the modified electrode were examined. The beneficial analytical characteristics of the proposed electrode were demonstrated. Our results indicate that the Gr/PTh/AuNPNTs/EDC–NHS/CAT_{pp} bioelectrode exhibits a wide linear range from 0.05 mM to 18.5 mM of H_2O_2, fast response time of 7 s, excellent sensitivity of 26.2 mA mM^{-1} cm^{-2}, good detection limit of 0.12 μM and good Michaelis–Menten constant of 1.4 mM. In addition, the bioelectrode displayed good repeatability, high stability and acceptable reproducibility, which can be attributed to the AuNPNTs–PTh composite that provides a biocompatible micro-environment.

Received 13th July 2014
Accepted 21st August 2014

DOI: 10.1039/c4an01262c

www.rsc.org/analyst

1. Introduction

Hydrogen peroxide (H_2O_2) is a well known oxidizing, bleaching and sterilizing agent. It is also one of the significant by-products or substrates of many biological reactions.[1,2] It plays an essential role in wastewater treatment, the paper and textile industries, and so on. Conversely, it has been recognized as a chemical threat in the progression of many diseases such as atherosclerosis, renal disease, ageing and others.[3] As a result, there is serious public concern for the selective, inexpensive and accurate determination of H_2O_2. A variety of methodologies have been developed for the quantification of H_2O_2, such as titrimetry, spectrometry, chemiluminescence and electrochemistry.[4–6] However, because of the relative merits and demerits of these analytical techniques, the electrochemical method is considered to be the most amenable and is receiving substantial interest because its convenience, efficiency, low cost, and so on. A number of electrochemical biosensors have been developed based on the electrocatalysis and direct electron transfer between the electrode and an immobilized enzyme or protein such as horseradish peroxidase, hemoglobin, and so on.[7,8] Nevertheless, enzymatic electrochemical biosensors suffer from inherent problems such as instability to pH, temperature, and exposure to chemicals, elaborate immobilization procedure, high cost and easy distortion during fabrication, use and

[a]*Department of Chemistry and Research Centre, N.M.K.R.V. College for Women, Jayanagar, Bangalore 560 011, India. E-mail: sureshssmrv@yahoo.co.in; Fax: +91-80-22453665; Tel: +91-80-26654920*

[b]*Department of Energy Systems and Engineering, Daegu Gyeongbuk Institute of Science and Technology, Daegu 711-873, Republic of Korea*

[c]*Department of Biochemistry, Kuvempu University, Shankarghatta, Shimoga 577451, India. E-mail: bpniru@gmail.com*

[d]*Nuclear Agriculture and Biotechnology Division, Bhabha Atomic Research Centre, Mumbai 400 085, India. E-mail: jsmelo@barc.gov.in*

storage.[9] In addition, the use of hemoglobin has been limited because of the lack of a diverse electron transfer process because of its large protein size and inaccessibility of the redox centre, which is insulated from the conductive support by the peptide backbone.[10] To circumvent these problems, it would be desirable and interesting to develop an electrochemical biosensor based on novel biological materials such as bioelectrocatalysts that can transcend the limitations of enzymes/proteins.

Methylotrophic yeasts such as *Pichia pastoris* (*Pp*) are promising sources of redox enzymes in biotechnology.[11] They contain catalase (CAT), an important enzyme sequestered together with alcohol oxidase in peroxisomes.[12] However, *Pp* is always associated with about 200- to 400-fold higher catalase activity than that of alcohol oxidase. Studies have shown that CAT detected in *Pp* resembles the peroxisomal CAT A of *Saccharomyces cerevisiae,* which is well documented to contain mitochondrial CAT.[13] Active peroxisomal CAT [EC 1.11.1.6] of approximately 240 kDa is a homotetramer made up of four polypeptide chains each over 500 amino acids long and it contains four porphyrin hemes as a co-factor that allows the enzyme to decompose H_2O_2 into water and oxygen.[14]

In recent years, advances in bionanoelectrochemistry have centered on investigations of nanomaterials, especially noble metal nanoparticles because of their exquisite sensitivity in chemical and biological sensing.[15] Specifically, gold nanoparticles (AuNPs) have exhibited enormous interest among researchers because they give a high surface-to-volume ratio for efficient and friendly loading of biomolecules, and they permit high and rapid electron transfer between electroactive species and the electrode. A great number of efficient synthetic procedures including chemical or photochemical reduction,[16] electrochemical reduction,[17] biosynthesis,[18] and so on, are currently being employed for the formation of AuNPs. In addition, the sonochemical method[19] has proved to be a new route that has been receiving much interest and significance. It is an intensively used technique in material chemistry for rapidly generating novel materials with useful properties having smaller size and higher surface area than other methods.

Since the discovery of carbon nanotubes by Ijima,[20] intense research has been seen on the development of new one-dimensional nanostructures that can be synthesized in the form of nanotubes (NTs), nanowires, nanorods, and so on. In the last decade, numerous publications have reported on NTs of various kinds including carbon, metallic and polymeric. Furthermore, NTs have proved to be superior because of their blend of extraordinary properties such as nanometer dimensions, elongated geometry, defined cavity, possible control of size, and accessible inner and outer surfaces.[21] Various synthetic strategies such as hydrothermal synthesis, surfactant-assisted synthesis, and electroradiation have been established for the synthesis of NTs.[22] Mitchell *et al.* have pioneered a novel method called template synthesis for the production of NTs.[23] This method entails synthesizing the desired material within the pores of a nanoporous template by chemical or electrochemical deposition or polymerization.[24] The nanostructures formed (nanoparticles–nanotubes), which preserve the relevant morphological parameters, are then released from the porous matrix by template dissolution.

Because of the advantageous characteristics of thiophene and its derivatives, electrochemically or chemically generated polythiophene (PTh) has been utilized in the development of an electrochemical sensor. The electropolymerization of thiophene does not require any oxidizing or reducing agent and the film thickness can be maintained. PTh possesses high solubility, good conductivity (10–1000 S cm^{-1}) and excellent thermal stability.[25] There is widespread recognition that gold has a high affinity for sulfur groups. The possibility of integrating gold nanostructures with thiolated organic species, *i.e.*, inorganic–organic hybrid materials can provide good chemisorption with impressive analytical performance and these materials have been used significantly in applications such as sensors and catalysis. A large volume of research work has been devoted to AuNP modified thiophene composites.[26,27] However, to the best of our knowledge, an electrochemical biosensor based on *Pp* CAT immobilized on AuNPNTs–PTh hybrid has not been investigated before.

In this paper, a simple bioelectrode has been proposed for the first time using CAT derived from *Pp* (CAT_{pp}) for the electrochemical detection of H_2O_2. Ultrasound irradiation was employed as a preparative protocol for the synthesis of AuNPs, while the nanoporous alumina membrane was used as a template for the fabrication of AuNPNTs. Then the tubular nanostructures of gold were tethered onto the graphite (Gr) electrode *via* chemisorbed sulfur containing electropolymerized thiophene. The CAT_{pp} was immobilized onto the inorganic–organic hybrid (*i.e.*, AuNPNTs–PTh) *via* an 1-ethyl-3-(3-dimethylaminopropyl)-carbodiimide and *N*-hydroxysuccinimide (EDC–NHS) coupling reagent. The morphology and chemical composition of the biosensor developed (Gr/PTh/AuNPNTs/EDC–NHS/CAT_{pp}) were investigated using scanning electron microscopy (SEM) and energy dispersive X-ray analysis (EDX), respectively. The electrochemical characterization of the electrodes was evaluated by cyclic voltammetry (CV) and electrochemical impedance spectroscopy (EIS) techniques. The analytical performance of the modified electrode was investigated using CV, differential pulse voltammetry (DPV) and chronoamperometry. Chronocoulometry was carried out for determination of the diffusion coefficient of H_2O_2 on the bioelectrode. The proposed bioelectrode Gr/PTh/AuNPNTs/EDC–NHS/CAT_{pp} demonstrates excellent electrocatalytic activity towards H_2O_2 with high sensitivity. The factors influencing the electrocatalytic response of the biosensor were examined. In addition, the interference of ascorbic acid (AA), dopamine (DA) and uric acid (UA) on reduction of H_2O_2 was studied at the Gr/PTh/AuNPNTs/EDC–NHS/CAT_{pp} electrode. The proposed bioelectrode is cost-effective, easy to fabricate, and possesses long-term stability with anti-fouling properties.

2. Experimental section

2.1. Reagents and materials

The yeast *Pp* (NCIM, no. 3419) was procured from the National Collection of Industrial Micro-organisms (NCIM) (National

Chemical Laboratory, Pune, India). Gold(III) chloride hydrate ($HAuCl_4$), isopropanol, 3-aminopropyl trimethoxysilane (APTMS), sodium perchlorate ($NaClO_4$), EDC, NHS, AA, DA and UA were obtained from Sigma-Aldrich. Thiophene was purchased from Loba Chemie. H_2O_2 (30%) and trisodium citrate were purchased from Merck Ltd., and nanoporous alumina membrane (Anodisc, 0.2 μm) was obtained from Whatman. The PK-3 electrode polishing kit (0.05 mm aqueous polishing alumina and 1 mm polishing diamond) was procured from BAS Inc. (Tokyo, Japan). Phosphate buffered saline (PBS) was prepared from stock solutions of 0.1 M K_2HPO_4, 0.1 M KH_2PO_4 and 0.1 M KCl. All other chemicals used were of analytical reagent grade, unless otherwise mentioned, and were used without further purification. The electrolyte solutions were deoxygenated during electrochemical experiments by bubbling ultra-pure nitrogen through them for at least 10 min to produce a homogeneous mixture.

2.2. Apparatus

Electrochemical experiments such CV, DPV, chronoamperometry and EIS were performed with a VersaSTAT 3 (Princeton Applied Research, USA). Chronocoulometry (CC) experiments were carried out using a CH Instruments Inc. machine. The impedance spectra were further examined using the ZSimpWin version 3.20 simulation program (Princeton Applied Research). Ultrasound irradiation was performed using a QSonica Ultrasonic processor equipped with a Ti horn that enabled 20 kHz ultrasound to be generated. The physical morphology of the modified electrodes was characterized using SEM and EDX using an Hitachi S-4800 II field-emission scanning electron microscope with an accelerating voltage of 5 kV. All of the electrochemical experiments were carried out using a conventional three-electrode cell assembly consisting of a saturated calomel electrode (SCE) as the reference electrode, platinum wire as the auxiliary electrode and bare Gr or a CAT_{pp} modified electrode as the working electrode.

2.3. Preparation of CAT_{pp} suspension

The *Pp* cells were sub-cultured on malt extract yeast peptone media at 28 °C containing 0.3 g malt extract, 1 g glucose, 0.3 g yeast extract, 0.5 g peptone, 2 g agar, and 100 mL distilled water, at pH 6.4–6.8. The activity of CAT_{pp} was monitored spectrophotometrically by measuring, every 15 s at room temperature (RT), the decrease in absorbance at 240 nm caused by the degradation of H_2O_2 using a molar extinction coefficient of 40.67 M^{-1} cm^{-1}.[28] The assay mixture contained 50 mM PBS, 30 mM H_2O_2 and 50 μL of cell free extract in a total volume of 1 mL. The amount of enzyme required to degrade 1 μM of H_2O_2 per minute under standard conditions was defined as 1 enzyme unit of the CAT activity and the results were expressed in U (μM H_2O_2 min^{-1} mL^{-1}). The activity of the CAT_{pp} was 24.6 U (in 50 μL of cell free extract) and it was chosen as the model bioelectrocatalyst for the fabrication of our proposed biosensor. For the preparation of the cell suspension, a loop full of the inoculum was suspended in 1 mL of buffer solution at pH 7. Subsequently, it was subjected to ultrasonic disruption for about 5 min to remove the permeability barriers between the intracellular CAT enzyme and the cell wall/membrane. The cell debris was removed by centrifugation and the supernatant solution was retained for the fabrication of the electrode.

2.4. Synthesis of AuNPs

AuNPs were prepared according to a previously reported sonochemical procedure[29,30] with a slight modification. In a typical procedure, 0.05 g of $HAuCl_4$ was dissolved in 300 mL of distilled water in a 500 mL beaker. In addition, 0.2 mM of isopropanol was also added to act as a radical scavenger and reaction accelerator. This solution was purged with argon for about 20 min to eliminate trace amounts of oxygen and to promote radical formation ($H^{\bullet}$ and $OH^{\bullet}$) from water. Subsequently, the solution was subjected to ultrasonication at RT, and then 3.4 g of trisodium citrate was injected gradually to act as a stabilizing agent. The chemical effects of ultrasound are derived principally from acoustic cavitation, *i.e.*, formation, growth and implosive collapse of bubbles in the liquid. The collapse of such bubbles in the irradiated solution results in localized hot spots with extremely high temperature (>5000 K), pressure (>20 MPa) and high cooling rates (>10^7 K s^{-1}) in a very short life time.[31] In our preliminary attempt to synthesize AuNPs by the sonochemical method, the rate of reduction of an aqueous solution of $HAuCl_4$ as a function of irradiation time and input amplitude of ultrasound was determined. It was found that, as the amplitude was increased from 10 to 100 at a rate of 20, the rate of Au(III) reduction increased. However, it was apparent that, at a lower amplitude of ultrasound, the sonochemical reduction was 20 times slower with the completion of formation of AuNPs in about two hours. Therefore, an amplitude of 100 was chosen as the optimum parameter for our experiment, in which the formation of AuNPs required only 5–10 min of irradiation time as witnessed by the change in colour of the gold solution. To obtain the best results, sonication parameters such as an amplitude of 100 that delivered an input power of ≈90 W were used. Upon ultrasonic irradiation, the color of the irradiated solution changed from yellow to black and finally to an intense, characteristic ruby red within 5–10 min of the sonication process indicating the formation of the desired AuNPs.

2.5. Synthesis of AuNPNTs

In the first step, the nanoporous alumina membrane was cleaned 3–5 times with isopropanol in an ultrasonic bath to remove any existing impurities. For the synthesis of AuNPNTs, the nanoporous alumina membrane was modified with APTMS following a method reported in the literature[32] and the as-synthesized AuNP solution was filtered by vacuum suction through the amino derivatized pores of the alumina membrane.[21] Filling of the pores with AuNPs occurred spontaneously. The silyl groups react with hydroxyl groups on the alumina membrane walls, leaving the amine groups available for binding nanoparticles. A portion of AuNP solution (15 mL) was passed through the APTMS treated alumina membrane. It can be recognised visually that this amount of solution coming out of the membrane was colourless indicating that all of the

AuNPs had been strongly adsorbed onto the amino derivatized alumina template. It was observed in these experiments that, when passing higher amounts of NP solution through the membrane, they would appear colored suggesting that the pore walls of the sacrificial template were covered with bound AuNPs and there was no free space for binding of further AuNPs. After passing 15 mL of AuNP solution, the template was washed by passing a few milliliters of distilled water through it to ensure that the membrane was not blocked. The AuNPNTs were isolated from the alumina membrane by detaching the template by dissolution with 0.1 M NaOH for 3 h followed by centrifugation. The isolated AuNPNTs were washed sequentially with distilled water and finally dried at 75 °C in an oven for 12 h. The AuNPNTs so obtained were dispersed to a final concentration of 5 mg mL^{-1} in pure water and used for the fabrication of the bioelectrode.

2.6. Preparation of the bioelectrode

An electrode was made by inserting a Gr rod of 6 mm diameter into a Teflon cylinder having the same internal diameter and length of 6 cm. Electrical contact was established by inserting a copper wire through the centre of the Teflon cylinder. The surface of the Gr electrode was well polished to obtain a mirror finish, with a shiny surface using a PK-3 electrode polishing kit. It was then rinsed for several minutes and ultrasonicated sequentially with distilled water to remove any impurities followed by drying. Because the gold nanostructures can interact strongly with S-containing functional groups, the Gr surface was modified with a thin film of S-containing electroactive thiophene monomer prepared by electropolymerization. In general, the analytical sensitivity and reproducibility of any biosensor is determined by the surface of the modified electrode. Therefore, identification of the optimum concentration of enzyme or thiophene is a crucial aspect for bioelectrode fabrication. The influence of electropolymerization parameters such as the optimum monomer concentration, the optimum number of CV cycles used to form the polymer film and the optimum scan rate of electropolymerization were investigated. As shown in Fig. 1, the best results that presented the maximum peak current and a good peak profile in a 0.5 M thiophene concentration for 10 potential cycles at a scan rate of 50 mV s^{-1} were preferred for the preparation of modified electrodes. Then the electropolymerization of thiophene on the Gr electrode was achieved by immersing the electrode in 10 mL of 0.5 M thiophene dissolved in acetonitrile containing 0.12 g of $NaClO_4$ as dopant. Subsequently, it was subjected to cyclic scanning in the range of 0 to −1.1 V at a scan rate of 50 mV s^{-1} for 10 potential cycles which resulted in the formation of thin films of PTh on the Gr surface. The Gr/PTh electrode was rinsed with acetonitrile to remove any unreacted monomer and then dried at RT. Then, 10 μL of AuNPNT solution was dropped uniformly onto the electrode surface and dried at RT to obtain the Gr/PTh/AuNPNT modified electrode. Furthermore, in order to induce covalent coupling between the CAT_{pp} solution and the Au nanostructures, the electrode was modified by drop coating 5 μL of 20 mM NHS solution and 5 μL of 40 mM EDC solution and then dried at room temperature. In addition to optimizing the enzyme concentration, the current response of the enzyme modified electrode was determined with different amounts of CAT solution using CV. At low CAT concentration, *i.e.* at 6 μL, which is equal to 3 U, there were no redox peaks detected with a low peak current response whereas the best results with maximum peak current were obtained with a 5 U (10 μL) enzyme concentration. However, further increases in the enzyme concentration (10 U, 15 U and 20 U) resulted in a lower response indicating a diffusion problem. Therefore, the ideal enzyme concentrations (10 μL) were chosen for the fabrication of the bioelectrode. Finally, covalent immobilization was carried out by dropping 10 μL (approximately 5 U) of CAT_{pp} suspension onto the electrode followed by incubation at 4 °C for 30 min. The resultant Gr/PTh/AuNPNTs/EDC–NHS/CAT_{pp} bioelectrode was rinsed with pure water to remove any unbound or loosely attached CAT_{pp} and then used for the electrochemical detection of H_2O_2. For comparison, Gr/EDC–NHS/CAT_{pp} and Gr/PTh/EDC–NHS/CAT_{pp} electrodes were prepared in a similar fashion.

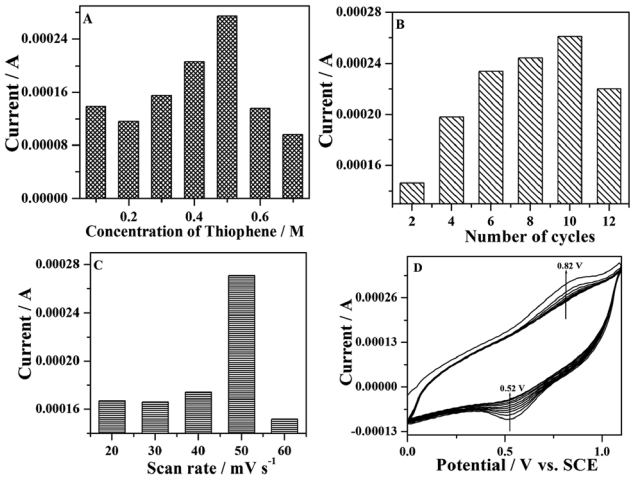

Fig. 1 Different electropolymerization parameters affecting the properties of the bioelectrode. (A) Effect of concentration of thiophene. (B) Effect of number of CV cycles. (C) Effect of scan rate of polymerization on the electrode. (D) Electropolymerization of thiophene on bare Gr electrode with optimized parameters.

3. Results and discussion

3.1. Structural characterization of AuNPs using UV-Vis spectroscopy, XRD and SEM

Ultraviolet-visible (UV-Vis) spectrophotometric analysis was carried using a Shimadzu UV-1700 UV-Vis spectrophotometer. The UV-Vis spectra recorded for the sonochemically reduced AuNPs are shown in Fig. 2A. A surface plasmon resonance (SPR) band centred at 525 nm is observed indicating the successful formation of AuNPs. In addition, it is well documented in the literature that the SPR band for spherical AuNPs usually occurs in the range between 520 and 530 nm.[33] This result indicates that spherical AuNPs were typically formed in our synthesis procedure. To investigate the size and crystalline structure of AuNPs, X-ray diffraction (XRD) measurements were made. The

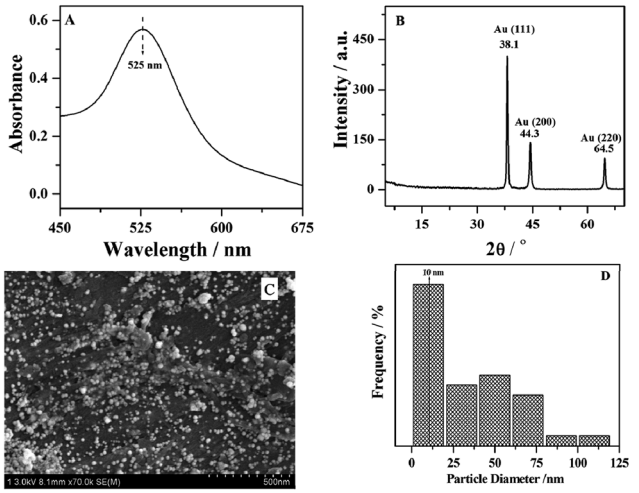

Fig. 2 (A) UV-Vis absorption spectra originating from SPR of AuNPs prepared by ultrasound irradiation. (B) XRD pattern of as-prepared AuNPs. (C) SEM images showing the spherical AuNPs obtained following sonochemical irradiation. (D) Typical particle diameter histogram.

powder XRD pattern (Fig. 2B) showed the appearance of sharp peaks at 2θ values of 38.1°, 44.3° and 64.5° which were indexed to the Au (111), (200), (220) planes, respectively, that can be assigned to the face-centred cubic structure of gold.[34] No other peaks characteristic of impurities can be observed showing the purity of the AuNPs. Furthermore, the particle size calculated for the crystalline nanoparticles using the Debye–Scherrer equation was found be 13.8 nm. The SEM image of AuNPs shown in Fig. 2C exhibits many spherical particles. It can be seen that the AuNPs are evidently individual entities. Particle size analysis of AuNPs was performed using ImageJ software (NIH) and the average diameter was 10 nm as illustrated in Fig. 2D. From these results, it can be concluded that the shape of the ultrasonically prepared AuNPs was spherical and their average particle diameter was 10 ± 2 nm.

3.2. Physical characterization of the modified electrodes using SEM and EDX

Fig. 3A shows the SEM image of a small piece of alumina template containing AuNPs before dissolution. It is seen that many AuNPs adhere to the porous template over the entire surface. Furthermore, the AuNPs synthesized by the sonochemical method were almost spherical in shape. This SEM image confirms the highly ordered arrangement of AuNPs within the pores of the templates leading to the formation of AuNPNTs. The Gr/PTh/AuNPNTs modified electrode shows the existence of a tubular morphology (Fig. 3A, inset) resulting from the sacrificial templates. It can be observed that the diameter of the AuNPNTs is approximately 200 nm. From the inset in Fig. 3A, one can infer that there is a homogenous distribution of AuNPNTs in the electrode composite. This indicates that PTh provides a suitable surface for the adherence of AuNPNTs onto the Gr surface by S–Au chemisorption. In comparison, the SEM image of the Gr/PTh/AuNPNTs/EDC–NHS/CAT_{pp} electrode (Fig. 3B) reveals the presence of several bright globular discrete particles. These particles can be attributed to the successful immobilization of large amounts of CAT_{pp} in the voids of the porous AuNPNT structure by EDC–NHS covalent coupling. The high surface coverage area and biocompatibility of AuNPNTs provide a good platform for the immobilization of large amounts of CAT_{pp}.

An elemental analysis was carried out to understand the chemical properties of the composites. The investigation of the nanoporous alumina membrane filled with AuNPs by EDX (Fig. 3C) revealed the presence of elemental Au, Al, C, O and Si signals. The Al and Si signals may be attributed to the alumina template. On the other hand, the EDX data obtained for the Gr/PTh/AuNPNTs electrode (Fig. 3D) shows the S signal arising from the thiophene despite the presence of Au, C and O. This gives an indication of S–Au chemisorption. However, the Gr/PTh/AuNPNTs/EDC–NHS/CAT_{pp} (Fig. 3E) illustrates a similar trend in the composition with the presence of Au, C, O and S together with the Fe anticipated for the CAT_{pp}. The detailed data for the weight percentage of the elements measured for each modified electrode are tabulated at the top of the corresponding figures (Fig. 3C–E).

3.3. Electrochemical characterization of the bioelectrode using CV and EIS using potassium ferricyanide

To investigate the ion accessibility of the modified electrodes, CVs of bare Gr, Gr/PTh, Gr/PTh/AuNPNTs and Gr/PTh/AuNPNTs/EDC–NHS/CAT_{pp} were obtained using 5 mM $Fe(CN)_6^{3-/4-}$ as the electrochemical probe. It is clear from Fig. 4A that the redox current for Gr/PTh (curve b) was superior to that of bare Gr (curve a) which may be, because of the good conductivity of PTh which can improve the electron transfer rate. When the electrode was modified further with AuNPNTs, the Gr/PTh/AuNPNTs electrode exhibited the highest peak current indicating that the AuNPNTs can act as tiny conducting centers accelerating the electron transfer and correspondingly enhancing the active electrode surface area. This validates the improved S–Au chemisorption formed between the inorganic and organic hybrid. However, the redox current clearly decreased after CAT_{pp} immobilization (curve d) indicating the sluggish electron transfer at the electrode surface because of the presence of an insulating enzyme layer. This proves the higher steric hindrance and successful immobilization of the enzyme in the nanocomposite. In addition, the peak-to-peak separation (ΔE_p) between the anodic and cathodic peaks decreased in the order: bare Gr ($\Delta E_p = 172$ mV) > Gr/PTh ($\Delta E_p = 169$ mV) > Gr/PTh/AuNPNTs ($\Delta E_p = 141$ mV) and Gr/PTh/AuNPNTs/EDC–NHS/CAT_{pp} ($\Delta E_p = 149$ mV). In addition, the voltammetric profiles (Fig. 4A) were subjected to quantitative mathematical analysis to elucidate the electroactive surface area. The active electrode area can be calculated according to the Randles–Sevcik equation as follows:[35]

$$I_p = 2.69 \times 10^5 A D^{1/2} n^{3/2} v^{1/2} C \quad (1)$$

where I_p is the peak current of the redox couple, A is the area of the electrode (cm^2), D is the diffusion coefficient ($cm^2\ s^{-1}$), n is

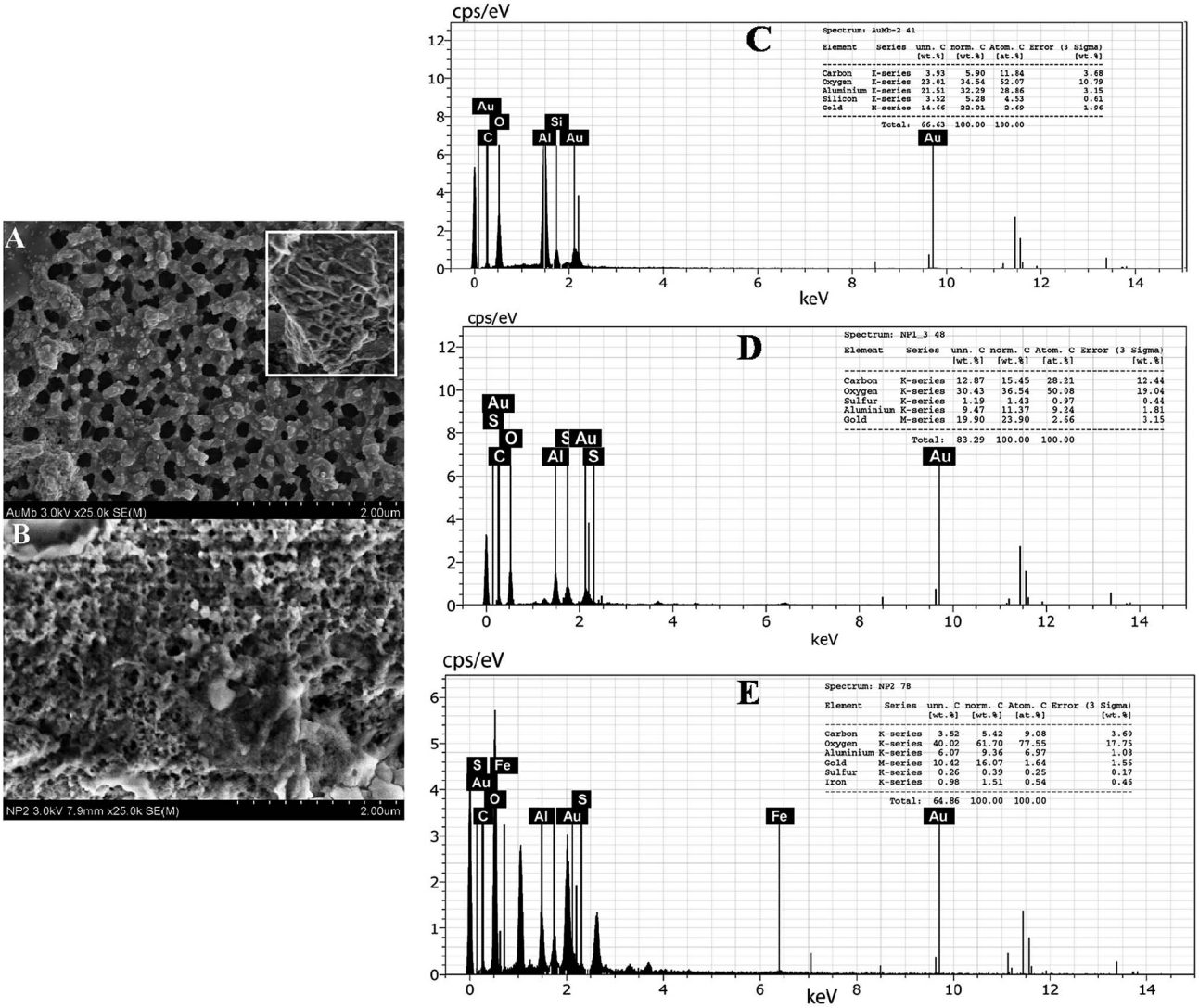

Fig. 3 SEM of (A) surface of 200 nm pore diameter alumina membrane comprising of coalesced AuNPs before membrane dissolution; inset is the SEM image of Gr/PTh/AuNPNTs after template dissolution. (B) Gr/PTh/AuNPNTs/EDC–NHS/CAT_{pp} modified electrodes. EDX patterns of (C) alumina template encompassing AuNPs, (D) Gr/PTh/AuNPNT electrode and (E) Gr/PTh/AuNPNTs/EDC–NHS/CAT_{pp} modified electrode. Insets are the quantitative results obtained from the EDX spectra of the corresponding electrodes.

the number of electrons participating in the redox reaction, υ is the scan rate (V s^{-1}) and C is the concentration of the probe molecule in the bulk solution (mol cm^{-3}). The order of calculated electroactive surface area was: bare Gr (0.167 cm^2) < Gr/PTh (0.175 cm^2) < Gr/PTh/AuNPNTs (0.231 cm^2) > Gr/PTh/AuNPNTs/EDC–NHS/CAT_{pp} (0.211 cm^2). It can be seen that the electroactive surface area of Gr/PTh/AuNPNTs electrode was increased by about 38.32% and 32% compared to that of bare Gr and Gr/PTh, respectively, which justifies the higher peak current achieved from the Gr/PTh/AuNPNT electrode and validates the evidence for the superior conductivity of AuNPNTs as was expected.

In addition, EIS experiments were also carried out to investigate the features of the electrode surface during each stepwise construction of the biosensor. EIS is found to be more consistent, efficient and precise than CV. A typical impedance spectrum represented in the form of Nyquist plots consists of a semicircular part and a linear part corresponding to the electron transfer limited process and the diffusion limited process, respectively. As shown in Fig. 4B, the redox process at the modified electrodes is controlled by both diffusion and electrochemical reactions. The diameter of the semicircular portion observed in the higher frequency range is equivalent to the electron transfer resistance R_{ct}. Its value can be used as a direct and sensitive parameter to depict the interfacial properties of surface-modified electrodes. The EIS experimental data obtained for the bare Gr (a), Gr/PTh (b), Gr/PTh/AUNPNTs (c) and Gr/PTh/AuNPNTs/EDC–NHS/CAT_{pp} (d) at frequencies varying from 0.1 Hz to 100 kHz are compared with an equivalent circuit (Fig. 4B, inset) that assists in understanding the electrical properties of the electrode/solution interface. It is noticeable that the circuit is composed of elements such as

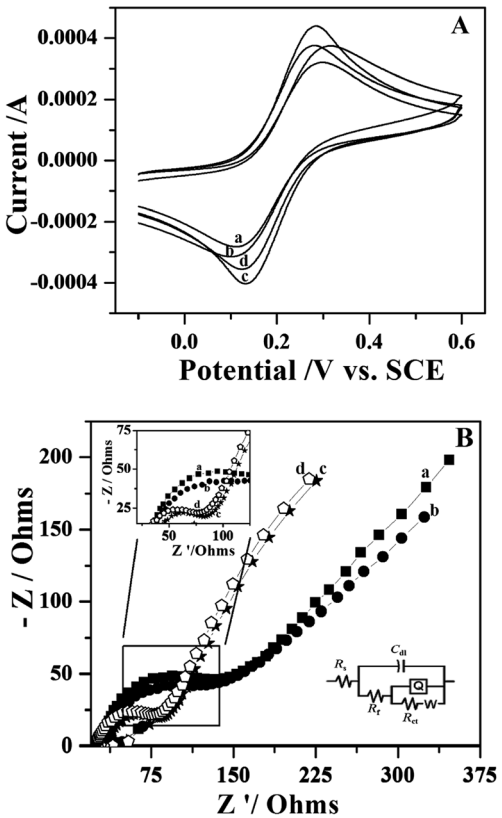

Fig. 4 (A) CVs obtained with the bare Gr (a), Gr/PTh (b), Gr/PTh/AuNPNTs (c), and Gr/PTh/AuNPNTs/EDC–NHS/CAT_{pp} (d) modified electrodes in 5 mM $Fe(CN)_6^{3-/4-}$ solution. (B) Nyquist relationships of EIS data for bare Gr (a), Gr/PTh (b), Gr/PTh/AuNPNTs (c) and Gr/PTh/AuNPNTs/EDC–NHS/CAT_{pp} (d) modified electrodes. Inset displays the equivalent circuit used in the fit procedure for impedance spectra.

solution resistance (R_s), double layer capacitance (C_{dl}), Faradic resistance (R_f), Warburg impedance (W) and R_{ct}. The best fitting impedance data obtained using the equivalent circuit is listed in Table 1. From Fig. 4B, it can be seen that the bare Gr electrode (curve a) manifested a large semicircle implying a high R_{ct} (65.92 Ω) of the redox probe which can be attributed to the poor catalytic activity of the Gr electrode. On the other hand, the Gr/PTh electrode depicts an R_{ct} of 52.34 Ω, which was reflected in a decreased semicircular part. This is apparently because of the improvement of the electric conductivity by the addition of the polymer. In comparison, after modification with AuNPNTs, the diameter of the semicircular part was found to decrease gradually with an R_{ct} of 41.38 Ω. This provides the evidence that the incorporation of AuNPNTs results in excellent electrical conductivity. In contrast, the CAT_{pp} modified bioelectrode showed hindered electron transfer with an increase in the R_{ct} value of 44.73 Ω which is in turn reflected by the increased semicircular part suggesting that the presence of CAT_{pp} can block the electron transfer kinetics, which was consistent with the CV results indicating the successful immobilization of CAT_{pp}.

Furthermore, it is well known that the electron transfer rate (k^0) for the ferricyanide system at the electrode surface decreases with increasing ΔE_p value.[36] Therefore, k^0 was calculated using the following equation:

$$R_{ct} = RT/(nF)^2 Ak^0C \quad (2)$$

where R_{ct} is the electron transfer resistance from the corresponding impedance plots of the modified electrodes, R is the ideal gas constant, T is the temperature, F is the Faraday constant, A is the area of the electrode, and C is the molar concentration of $Fe(CN)_6^{3-/4-}$. From eqn (2), the k^0 values for the bare Gr electrode, and the Gr/PTh, Gr/PTh/AuNPNTs and Gr/PTh/AuNPNTs/EDC–NHS/CAT_{pp} modified electrodes were 2.78×10^{-4}, 3.5×10^{-4}, 4.4×10^{-4} and 4.1×10^{-4} cm s^{-1}, respectively. The k^0 for the Gr/PTh/AuNPNT electrode was 58% times higher than for the bare Gr electrode and 26% times higher than for the Gr/PTh electrode in the same electrolyte solution indicating that the presence of AuNPNTs improved the conductivity and increased the electron transfer rate.

3.4. Comparison of the voltammetric response of the modified electrodes towards H_2O_2 reduction

To verify the efficacy of the proposed bioelectrode towards the detection of H_2O_2, the electrochemical reduction at the Gr/PTh/AuNPNTs/EDC–NHS/CAT_{pp} electrode was examined and compared with the other modified electrodes. Fig. 5A illustrates the CV results measured in nitrogen saturated solution in the presence of 4 mM H_2O_2 in the potential window 0 to −0.8 V at a scan rate of 50 mV s^{-1}. As can be seen, the current delivered at the Gr/EDC–NHS/CAT_{pp} electrode (curve a) is very small indicating the lack of a stable electroactive species. However, under identical conditions, the Gr/PTh/EDC–NHS/CAT_{pp} electrode (curve b) produced an increased peak current giving clear evidence for better conductivity, larger surface area and good electrocatalytic activity of PTh towards H_2O_2. In the presence of AuNPNTs without CAT_{pp}, there is a significant increment in the reduction current (curve c, Gr/PTh/AuNPNTs electrode)

Table 1 Impedance components for the Gr/PTh/AuNPNTs/EDC–NHS/CAT_{pp} electrodes determined by fitting EIS experimental data using the equivalent circuit

Electrode	R_s (Ω)	C_{dl} (F)	n	R_{ct} (Ω)	R_f (Ω)	W (Ω)
Bare Gr	34.84	2.95×10^{-5}	0.5	65.92	134.7	0.0018
Gr/PTh	36.68	2.58×10^{-5}	0.8	52.34	4.07×10^{8}	1.66×10^{-14}
Gr/PTh/AuNPNTs	39.98	5.47×10^{-5}	0.8	41.38	4.765	1.079
Gr/PTh/AuNPNTs/EDC–NHS/CAT_{pp}	28.92	5.21×10^{-5}	0.6	44.73	218.3	0.0004

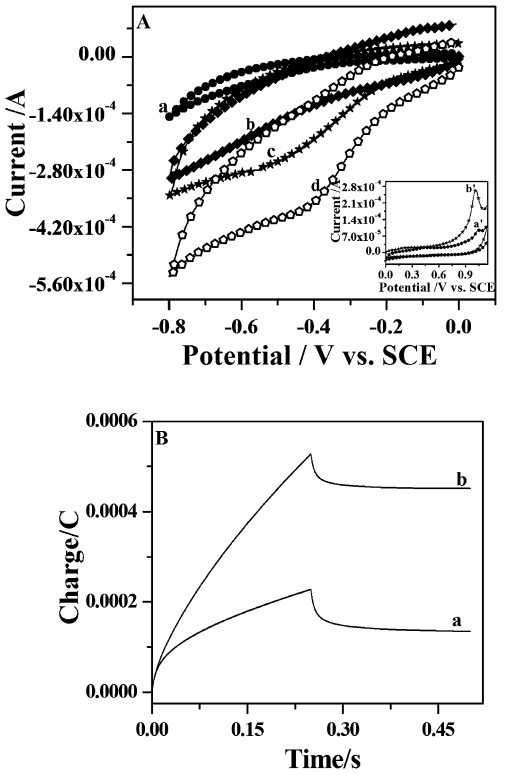

Fig. 5 (A) CVs of 5 mM H_2O_2 at (a) Gr/EDC–NHS/CAT_{pp}, (b) Gr/PTh/EDC–NHS/CAT_{pp}, (c) Gr/PTh/AuNPNTs and (d) Gr/PTh/AuNPNTs/EDC–NHS/CAT_{pp} electrode in 0.1 M PBS with a scan rate of 50 mV s^{-1}. (B) Chronocoulometric responses of the Gr/PTh/AuNPNTs/EDC–NHS/CAT_{pp} electrode in (a) the absence and (b) the presence of 2 mM H_2O_2 in 0.1 M nitrogen saturated PBS solution.

compared with the two earlier electrodes which confirms that the effective surface area of the electrode is efficiently enhanced using a Au nanostructure composite.

Before immobilization of CAT_{pp} onto the inorganic–organic hybrid (*i.e.*, AuNPNTs and PTh), we examined the superiority of AuNPNTs over AuNPs. To support the information, CVs were recorded for the Gr/PTh/AuNPs (a′) electrode in the presence of 2 mM H_2O_2 and compared with the Gr/PTh/AuNPNTs (b′) electrode. It is clear from the inset in Fig. 5A that the Gr/PTh/AuNPNTs electrode demonstrates better electrocatalytic activity (approximately 1.5-fold increased current) towards H_2O_2 because of its higher surface to volume ratio compared to the Gr/PTh/AuNPs electrode where AuNPs act as tiny conducting wires and offer more binding sites for the molecules allowing the loading of a large number of enzyme molecules thus enhancing the electrocatalytic response to H_2O_2. The proposed bioelectrode (curve d) showed a 1.5-fold higher electrocatalytic response to H_2O_2 than the AuNPNTs modified electrode and a 2.4-fold higher current response than the PTh modified electrode at a more positive potential. Apparently, the Gr/PTh/AuNPNTs/EDC–NHS/CAT_{pp} displayed a pair of quasi-reversible redox peaks of the $Fe^{(III)}/Fe^{(II)}$ redox couple characteristic of the CAT with a formal potential E^0 of −0.322 V which was slightly more positive than the −0.414 V reported for the single-walled carbon nanotube–Au modified electrode with CAT.[37] This positive shift in E^0 could be because of the components of the electrode that affect the electrostatic double layer. Based on these experimental observations, we can deduce that AuNPNTs act as an electron transfer facilitator from the redox species of CAT to the electrode surface. The tubular gold nanostructures assist in accommodating a greater number of CAT molecules in a favorable orientation in the vicinity of the electrode. The integration of AuNPNTs–PTh (inorganic–organic hybrid) improves the conductivity, lowers the overpotential for H_2O_2 reduction and offers a biocompatible microenvironment for CAT_{pp}. Accordingly, it is worth noting that CAT_{pp} (where only 5 U of enzyme has been used) can be a good preference for the fabrication of an H_2O_2 sensor and it is superior to the reported literature value of 200 U for CAT from bovine liver.[38]

3.5. Determination of the diffusion coefficient and adsorption of H_2O_2 on the Gr/PTh/AuNPNTs/EDC–NHS/CAT_{pp} bioelectrode using CC

Chronocoulometry is one of the most conventional electrochemical techniques used in electroanalytical chemistry. It is the measurement of charge as a function of time. The CC technique was applied to determine the diffusion coefficient (D) and Q_{ads} of H_2O_2 on the proposed electrode using the Anson equation:[39]

$$Q = \frac{2nFACDt^{1/2}}{\pi^{1/2}} + Q_{dl} + Q_{ads} \quad (3)$$

where n represents the number of electrons transferred in the electrochemical reaction, F is the Faraday constant, A is the area of the electrode in cm^2, D is the diffusion coefficient ($cm^2\ s^{-1}$), t is the time (ms), Q_{dl} is the double layer charge and Q_{ads} is the adsorption charge. Two series of CC experiments were performed, first using the Gr/PTh/AuNPNTs/EDC–NHS/CAT_{pp} electrode in the presence of 2 mM H_2O_2 and then the same electrode in the supporting electrolyte in the absence of electroactive species. Typical CC responses, *i.e.*, plot of charge as a function of time are given in Fig. 5B. The CC responses of the modified electrode in the presence and absence of H_2O_2 were then converted to Anson plots by plotting Q *vs.* $t^{1/2}$. The Anson plot shows a linear relationship of Q with $t^{1/2}$ indicating a diffusion controlled electrochemical process. From the slope and intercept of the linear relationship, the parameters D and Q_{ads} were calculated using the eqn (3). Accordingly, D and Q_{ads} were estimated to be 6.1×10^{-5} $cm^2\ s^{-1}$ and 6.69×10^{-5} C, respectively. In addition, the surface concentration Γ_s was calculated using eqn (4) and it was found to be 12.5×10^{-10} mol cm^{-2}:

$$\Gamma_s = \frac{Q_{ads}}{nFA} \quad (4)$$

3.6. Electrocatalytic properties of the H_2O_2 biosensor

The electrocatalytic reduction of H_2O_2 at the proposed bioelectrode was studied in the absence and presence of varying concentrations of the analyte in 0.1 M PBS (pH 7). Fig. 6A shows CVs obtained in the potential window 0 to −0.8 V at a scan rate of 50 mV s^{-1}. In the absence of H_2O_2, a pair of redox peaks was

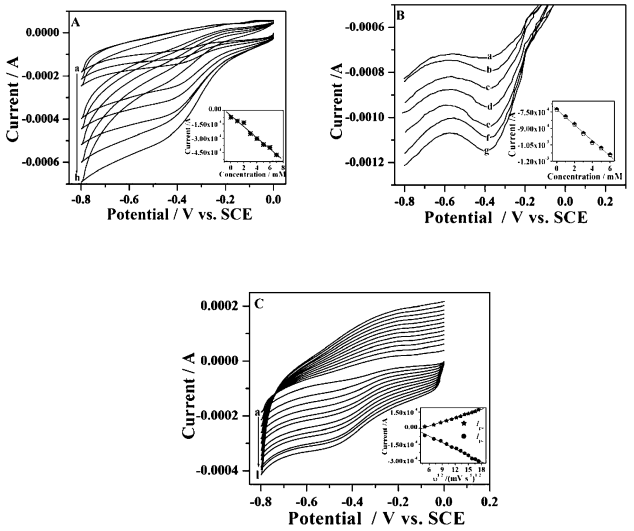

Fig. 6 (A) CV responses of the Gr/PTh/AuNPNTs/EDC–NHS/CAT_{pp} electrode for different concentrations (a–h: 0, 1, 2, 4, 5, 6, 7 and 8 mM) of H_2O_2 in 0.1 M nitrogen saturated PBS solution. Inset is the plot of peak current against added H_2O_2 concentration. (B) DPV curves obtained upon stepwise addition of increasing concentrations (a–g: 0, 1, 2, 3, 4, 5 and 6 mM) of H_2O_2 in neutral 0.1 M PBS for the proposed Gr/PTh/AuNPNTs/EDC–NHS/CAT_{pp} electrode. Inset is the concentration dependence of the peak currents obtained from the DPV measurements. (C) CVs of 2 mM H_2O_2 at the Gr/PTh/AuNPNTs/EDC–NHS/CAT_{pp} electrode at different scan rates (a–l: 25, 50, 75, 100, 125, 150, 175, 200, 225, 250, 275 and 300 mV s^{-1}). Inset is the dependence of the anodic and cathodic peak current on the square root of scan rate.

observed at −0.252 V (E_{pa}) and −0.370 V (E_{pc}), and is characteristic of the $Fe^{(III)}/Fe^{(II)}$ redox couple of CAT. Upon sequential addition of 1 mM H_2O_2, the voltammetric peak corresponding to the electrocatalytic reduction of H_2O_2 increased gradually at −0.370 V accompanied by a decrease in oxidation current indicating a typical electrocatalytic process at the Gr/PTh/AuNPNTs/EDC–NHS/CAT_{pp} electrode. After addition of a two-fold concentration of H_2O_2, the cathodic peak was found to increase correspondingly suggesting that the catalytic current of the bioelectrode was determined by the concentration of H_2O_2. The electrocatalytic mechanism can be expressed as follows:

$$\text{CAT–Fe(III)} + e^- + H^+ \leftrightarrow \text{CAT–Fe(II)}H^+ \text{ at the electrode surface} \quad (5)$$

$$H_2O_2 + \text{CAT–Fe(II)}\ H^+ \rightarrow \text{CAT–Fe(III)} + H^+ + H_2O \text{ in solution} \quad (6)$$

here, CAT–Fe(III) and CAT–Fe(II) represent the oxidized and reduced forms of CAT, respectively. From the mechanism, it can be seen that, when CAT–Fe(III) undergoes electron transfer reaction with the electrode, CAT–Fe(II)H^+ can be oxidized by H_2O_2 in the solution to regenerate CAT–Fe(III). This electrode reaction differs slightly from the conventional E_rC_i' mechanism in that both the CAT–Fe(III) and CAT–Fe(II)H^+ are surface confined. A typical calibration plot of electrocatalytic current *versus* concentration of H_2O_2 for the Gr/PTh/AuNPNTs/EDC–NHS/CAT_{pp} electrode is shown in Fig. 6A (inset). As revealed in the inset, the cathodic peak current (I_{pc}) was linear with concentrations of H_2O_2 in the range 0 to 8 mM and its linear regression equation is given next:

$$I_{pc} = -5.805 \times 10^{-5} - 5.927 \times 10^{-5}\, C_{H_2O_2}\,(\text{mM});\ R = -0.990 \quad (7)$$

DPV has the advantage of having higher current sensitivity and better resolution compared to CV, therefore, the detection of various concentrations of H_2O_2 using the proposed electrode was investigated using DPV in the potential range of 0 to −0.8 V. As for the CV analysis, DPV measurements were first obtained in the absence of H_2O_2, followed by the analysis of increasing concentrations of H_2O_2. It is apparent from Fig. 6B that the dependence of the reduction peak current was linear (inset Fig. 6B) with a concentration of H_2O_2 in the range 0 to 6 mM. The linear regression equation is as follows:

$$I_{pc} = -7.270 \times 10^{-4} - 7.085 \times 10^{-4}\, C_{H_2O_2}\,(\text{mM});\ R = -0.997 \quad (8)$$

To elucidate the kinetics of the electrode reaction of H_2O_2 detection at the electrode surface, the effect of scan rate on the peak current at the modified electrode was investigated using 2 mM H_2O_2 and the results are shown in Fig. 6C. As expected, the overlaid CVs of the Gr/PTh/AuNPNTs/EDC–NHS/CAT_{pp} electrode illustrate an increase in oxidation and reduction in peak current with the increase in the scan rate from 25 to 300 mV s^{-1}. A good linear relationship between the peak currents and the square root of scan rate was achieved as shown in the inset of Fig. 6C with the linear regression equation as specified next:

$$I_{pa} = 7.672 \times 10^{-6} + 5.629 \times 10^{-7}\, \upsilon^{1/2}\,(\text{V s}^{-1});\ R = 0.995 \quad (9)$$

$$I_{pc} = -5.529 \times 10^{-5} - 8.660 \times 10^{-7}\, \upsilon^{1/2}\,(\text{V s}^{-1});\ R = -0.995 \quad (10)$$

All of these characteristics suggest that the electrochemical reaction occurring at the Gr/PTh/AuNPNTs/EDC–NHS/CAT_{pp} electrode is a diffusion controlled process.

3.7. Influence of applied potential, temperature and pH on the Gr/PTh/AuNPNTs/EDC–NHS/CAT_{pp} bioelectrode

To improve the performance of the biosensor, an assortment of working parameters such as applied potential, temperature and pH that play an important role were optimized.

The selection of the operating potential on the working electrode is useful in achieving high sensitivity, the best detection limit and good selectivity of the system in avoiding electroactive interfering species. In order to evaluate the effect of applied potential, the electrocatalytic reduction of H_2O_2 was examined at the Gr/PTh/AuNPNTs/EDC–NHS/CAT_{pp} electrode by chronoamperometry over the potential range of −200 to −450 mV. Amperometric measurements were recorded under stirring conditions by sequentially injecting 2 mM H_2O_2 for a period of 300 s. Fig. 7A shows a plot of operating potential *vs.* electrocatalytic peak current response to the successive addition of

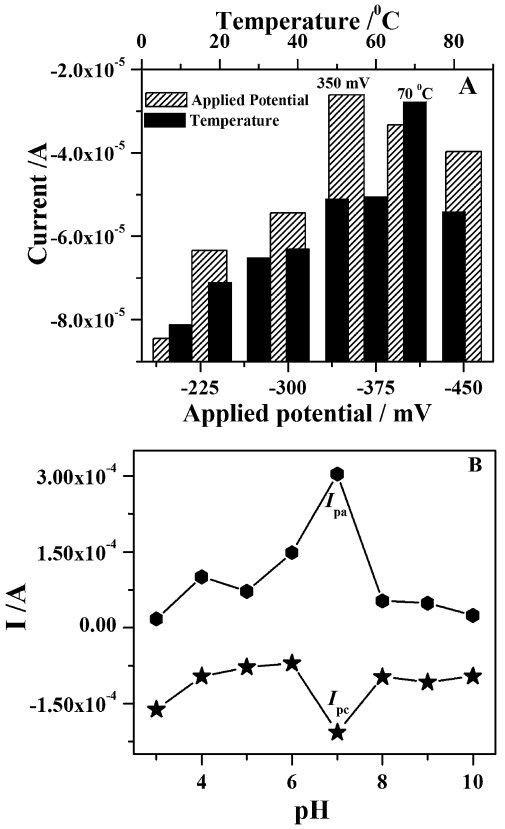

Fig. 7 (A) Effect of operating potential (hatched bars) and temperature (solid bars) on the CV response of the modified electrode to 2 mM H_2O_2. (B) Dependence of anodic and cathodic peak currents of 2 mM H_2O_2 on pH values (3 to 10) of the solution at the Gr/PTh/AuNPNTs/EDC–NHS/CAT_{pp} electrode.

H_2O_2. As can be seen, in the potential range studied, we can interpret that the reduction of H_2O_2 starts at −200 mV and increases appreciably towards the negative potential reaching a plateau at −350 mV. However, with a more negative increase in potential, the peak current decreased revealing that the proposed electrode has better electrocatalytic activity for the reduction of H_2O_2 at −350 mV. Consequently, to achieve the highest sensitivity and to avoid interference, an applied potential of −350 mV (*vs.* SCE) was chosen for all further experiments.

Furthermore, the effect of temperature on the biocatalytic response of the bioelectrode by CV in the presence of a constant H_2O_2 concentration of 2 mM was investigated. Fig. 7A shows the trend of the variation of electrocatalytic peak response of the Gr/PTh/AuNPNTs/EDC–NHS/CAT_{pp} electrode as a function of temperature. As depicted, by increasing the temperature from 10 °C, the catalytic current increases to achieve its maximum value at 70 °C. A decrease in current can be observed when the temperature exceeds 70 °C indicating partial denaturation of the enzyme at higher temperatures. This increase in thermal stability can be attributed to the beneficial effect brought about by the AuNPNTs–PTh hybrid that provides good biocompatibility to the immobilized enzyme. Nevertheless, considering the lifetime and characteristic electrocatalytic response of the bioelectrode, all subsequent experiments were performed at RT.

To determine the pH stability of the Gr/PTh/AuNPNTs/EDC–NHS/CAT_{pp} electrode, the dependence of the solution pH on the voltammetric response of the bioelectrode was scrutinized in the pH range 3 to 10 (standard buffer solutions) in the presence of a constant H_2O_2 concentration of 2 mM. According to the pH profile depicted in Fig. 7B, the peak current increases with increasing pH reaching a maximum at pH 7 and declines afterwards up to pH 10. Consequently, pH 7 was chosen as the optimum pH with a maximum activity of the enzyme constituents immobilized on the bioelectrode, which is consistent with the results previously reported in the literature[40] indicating that the electrode composite offers a biocompatible microenvironment for CAT.

3.8. Chronoamperometric response of the Gr/PTh/AuNPNTs/EDC–NHS/CAT_{pp} bioelectrode

The chronoamperometric current response of the proposed bioelectrode was measured in 0.1 M nitrogen saturated PBS solution under the optimal experimental conditions. Fig. 8A illustrates a typical current *versus* time plot for the Gr/PTh/AuNPNTs/EDC–NHS/CAT_{pp} electrode that was evaluated with the stepwise addition of various amounts of H_2O_2 to a stirred electrolyte solution at a static potential of −350 mV (*vs.* SCE). A

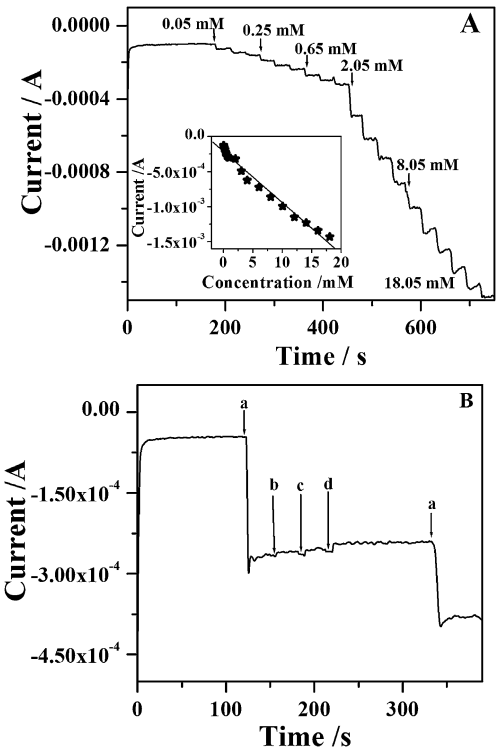

Fig. 8 (A) Typical amperometric current response for the Gr/PTh/AuNPNTs/EDC–NHS/CAT_{pp} electrode upon successive additions of various concentrations of H_2O_2 at an applied potential of −350 mV (*vs.* SCE) in 0.1 M PBS solution. Inset is the calibration plot of current *versus* H_2O_2 concentration. (B) The amperometric response of the modified bioelectrode to successive additions of 2 mM H_2O_2 (a) and interferences 200 μM DA (b), 1 mM AA (c) and 0.5 mM UA (d) in 0.1 PBS at pH 7 and an applied potential of −350 mV.

rapid co-relative amperometric current response of approximately 7 s was attained at every 30 s aliquot of H_2O_2 addition indicating a fast electron transfer. From the steady-state amperograms, a calibration plot was made using current as a function of concentration and the results are shown in Fig. 8A (inset). The electrode exhibited a wide linear range between 0.05 mM and 18.5 mM with a correlation coefficient of −0.991, detection limit of 0.12 μM (at a signal-to-noise ratio of 3) and sensitivity of 26.2 mA mM^{-1} cm^{-2}. At a higher concentration range, the electrocatalytic response of the bioelectrode tends to become a plateau illustrating a characteristic Michaelis–Menten kinetic mechanism. The Michaelis–Menten constant (K_M) gives an indication of the enzyme-substrate kinetics and can be estimated from the electrochemical analogue of the Lineweaver–Burk equation[41] as follows:

$$1/I_{ss} = 1/I_{max} + K_M/I_{max}C \quad (11)$$

where I_{ss} is the steady-state current after the addition of the substrate, C is the bulk concentration of the substrate and I_{max} is the maximum current measured under saturated substrate conditions. From the plot of $1/I_{ss}$ *vs.* $1/C$, the K_M value can be estimated using the slope and intercept for the proposed bioelectrode. The K_M value for the Gr/PTh/AuNPNTs/EDC–NHS/CAT_{pp} electrode was calculated to be 1.4 mM, which was less than 40.7 mM for CAT immobilized on a glassy carbon electrode (GCE) by poly(glycidylmethacrylate-*co*-vinylferrocene)[42] signifying the good enzyme activity, strong binding of the immobilized CAT_{pp} on AuNPNTs–PTh composite, and its high affinity for H_2O_2 detection. The beneficial analytical characteristics of our proposed bioelectrode were compared with other previously reported non-enzymatic, horseradish peroxidase (HRP) and CAT-based H_2O_2 sensors[38,42–46] and the results are presented in Table 2. As summarized in the table, the Gr/PTh/AuNPNTs/EDC–NHS/CAT_{pp} electrode displayed superior analytical data to those documented in the literature.

3.9. Effect of interferents on the Gr/PTh/AuNPNTs/EDC–NHS/CAT_{pp} bioelectrode

To fulfill the practical applicability of the biosensor, a selectivity study is obligatory for any biosensors developed. The influences of some of the common electroactive species that are known to interfere with H_2O_2 detection have been investigated as shown in Fig. 8B. The low operating potential −350 mV (*vs.* SCE) given by the Gr/PTh/AuNPNTs/EDC–NHS/CAT_{pp} electrode significantly curtails the effect of interferents such as AA, UA and DA which are commonly present in biological samples. The normal concentration ranges of AA, UA and DA are 34–79 mM, 0.18–0.42 mM, and 1 μM, respectively.[47] The amperometric response obtained in the presence of 2 mM H_2O_2: (a) shows a well defined stable current response. Alternatively, the contributions of subsequent additions of 200 μM DA (b), 1 mM AA (c) and 0.5 mM UA (d), higher than the normal physiological concentrations, are negligible indicating that the Gr/PTh/AuNPNTs/EDC–NHS/CAT_{pp} electrode has good selectivity for H_2O_2. The integration of AuNPNTs–PTh (inorganic–organic hybrid) lowers the overpotential for H_2O_2 reduction and allows us to overcome the potential interference.

3.10. Stability and reproducibility tests for the Gr/PTh/AuNPNTs/EDC–NHS/CAT_{pp} bioelectrode

The repeatability, stability and reproducibility of the Gr/PTh/AuNPNTs/EDC–NHS/CAT_{pp} bioelectrode are essential factors for its practical application. The repeatability of the proposed bioelectrode was investigated with a series of repetitive measurements carried out with the same modified electrode in the presence of 3 mM H_2O_2 in nitrogen saturated 0.1 M PBS solution. The results of 21 successive CV measurements showed that the bioelectrode could retain 95% of its initial current response indicating that the modified bioelectrode had good repeatability and the ability to withstand fouling. Furthermore, the long-term stability (shelf life) was also tested over a four week period. The electrocatalytic response of the fabricated electrode was verified by consecutive potential scans in the presence of 2 mM H_2O_2. The magnitude of the current response measured under identical conditions decreased by approximately 1.2% of its initial value after one week and by 4.2% after four weeks indicating that the electrode was stable for H_2O_2 detection. The bioelectrode was cleaned with CV cycles in PBS after each measurement to eradicate the adsorption of the analyte and it was stored at 4 °C. In addition, the electrode capability to generate a reproducible surface was also examined using six different modified electrodes fabricated using the same procedure. These six electrodes exhibited a comparable electrocatalytic response to 3 mM H_2O_2 with an relative standard deviation of 3.1% obtained under optimum conditions, which confirmed that reproducible results could be obtained using the Gr/PTh/AuNPNTs/EDC–NHS/CAT_{pp} bioelectrode.

Table 2 Comparison of the analytical data obtained by the proposed electrode with data from other electrochemical H_2O_2 sensors

H_2O_2 electrochemical sensor	Response time (s)	Linear range (mM)	Detection limit (μM)	Sensitivity (mA mM^{-1} cm^{-2})	Reference
MWCNTs–Nf–(DDAB/CAT)	5	0.36–5.42	0.9	0.101	38
CAT/poly(GMA-*co*-VFC)	<6	0.5–14	80	0.000034	42
Nf/CAT/ERGO	5	0.05–1.91	—	0.0077	43
Iron oxide–silver hybrid modified GC electrode	3	0.0012–3.5	1.2	—	44
Ta–C–P/Au_2 electrode	8	0.0002–1	0.08	0.00029	45
HRP/GE–CNT–Nafion/AuPt NPs/GCE	—	0.0005–0.1	0.17	0.370	46
Gr/PTh/AuNPNTs/EDC–NHS/CAT_{pp}	7	0.05–18.5	0.12	26.2	This work

These results demonstrate that the proposed bioelectrode has good repeatability, high stability and good reproducibility, which may be ascribed to the excellent biocompatible microenvironment offered by the AuNPNTs–PTh (inorganic–organic hybrid) that conserves CAT_{pp} from antifouling and denaturation.

4. Conclusion

In an effort to develop a highly sensitive electrochemical H_2O_2 biosensor, we present the use of CAT_{pp} as a bioelectrocatalyst in the fabrication of a sensor. We have successfully synthesized AuNPs through sonochemical reduction of $HAuCl_4^-$. The template synthesis method was used to prepare AuNPNTs that offer a high surface area to volume ratio. The modification of the Gr surface with an electropolymerized film of thiophene provided S groups that allow strong binding of AuNPNTs onto the Gr surface. The integration of S–Au gives an effective immobilization platform to fabricate a novel H_2O_2 biosensor. Investigations of the modified electrode clearly revealed that the proposed electrode showed enhanced electrocatalytic activity towards H_2O_2 reduction at a potential of approximately −350 mV (*vs.* SCE), less positive than the bare Gr electrode. The biosensor possesses the function of AuNPNTs and PTh that can facilitate electron transfer, accommodate a greater number of enzyme molecules, provide a biocompatible microenvironment, lower the reduction potential and improve the conductivity. Furthermore, the AuNPNTs–PTh modified CAT_{pp} immobilized bioelectrode illustrates some excellent characteristics such as rapid response, wide linear range, low detection limit, excellent selectivity, good repeatability, long-term stability, good reproducibility, anti-fouling properties, and low cost with easy fabrication. It can be concluded from the experimental results that the proposed bioelectrode could be an alternative to existing expensive enzymatic methods used for the detection of H_2O_2.

Acknowledgements

The authors gratefully acknowledge the financial assistance from the Department of Atomic Energy – Board of Research in Nuclear Sciences, Government of India. We also thank Sri. A.V.S. Murthy, honorary secretary, Rashtreeya Sikshana Samiti Trust, Bangalore and Dr Shanta Sastry, Principal, NMKRV College for Women, Bangalore for their continuous support and encouragement. Part of this work was supported by the DGIST R&D Program of the Ministry of Education, Science and Technology of Korea (14-BD-01).

References

1 A. Salimi, R. Hallaj, S. Soltanian and H. Mamkhezri, *Anal. Chim. Acta*, 2007, **594**, 24–31.
2 Y. Usui, K. Sato and M. Tanaka, *Angew. Chem., Int. Ed.*, 2003, **42**, 5623–5625.
3 C. D. Bryan and J. C. Christopher, *J. Am. Chem. Soc.*, 2008, **130**, 11561.
4 W. P. Lian, L. Wang, Y. H. Song, H. Z. Yuan, S. C. Zhao, P. Li and L. L. Chen, *Electrochim. Acta*, 2009, **54**, 4334–4339.
5 B. Wang, J. J. Zhang, Z. Y. Pan, X. Q. Tao and H. S. Wang, *Biosens. Bioelectron.*, 2009, **24**, 1141–1145.
6 L. Wenjuan, Y. Ruo, C. Yaqin, Z. Lu, C. Shihong and L. Na, *J. Biochem. Biophys. Methods*, 2008, **70**, 830–837.
7 S. Nalini, S. Nandini, S. Shanmugam, S. E. Neelagund, J. S. Melo and G. S. Suresh, *J. Solid State Electrochem.*, 2014, **18**, 685–701.
8 L. Zhang, *Biosens. Bioelectron.*, 2008, **23**, 1610–1615.
9 X. Miao, R. Yuan, Y. Chai, Y. Shi and Y. Yuan, *J. Electroanal. Chem.*, 2008, **612**, 157–163.
10 X. Zeng, W. Wei, X. Li, J. Zheng and L. Wu, *Bioelectrochemistry*, 2007, **71**, 135–141.
11 M. Veenhuis and J. Goodman, *J. Cell Sci.*, 1990, **96**, 583–590.
12 P. E. Purdue and P. B. Lazarow, *Annu. Rev. Cell Dev. Biol.*, 2001, **17**, 701–752.
13 D. Koleval, V. Petroval, T. Hristozova and A. Kujumdzieva, *Biotechnol. Biotechnol. Equip.*, 2008, **22**, 762–768.
14 I. J. Van-der-Klei, H. Yurimoto, Y. Sakai and M. Veenhuis, *Biochim. Biophys. Acta*, 2006, **1763**, 1453–1462.
15 A. Moores and F. Goettmann, *New J. Chem.*, 2006, **30**, 1121–1132.
16 J. Polte, T. T. Ahner, F. Delissen, S. Sokolov, F. Emmerling, A. F. Thunemann and R. Kraehnert, *J. Am. Chem. Soc.*, 2010, **132**, 1296–1301.
17 N. Toshima, T. Yonezawa and K. Kushihashi, *J. Chem. Soc., Faraday Trans.*, 1993, **89**, 2537–2543.
18 M. A. Faramarzi and H. Forootanfar, *Colloids Surf., B*, 2011, **87**, 23–27.
19 Y. Nagata, Y. Mizukoshi, K. Okitsu and Y. Maeda, *Radiat. Res.*, 1996, **146**, 333–338.
20 S. Ijima, *Nature*, 1991, **354**, 56–58.
21 T. Sehayek, M. Lahav, R. Popvitz-Biro, A. Vaskevich and I. Rubinstein, *Chem. Mater.*, 2005, **17**, 3743–3748.
22 C. N. R. Rao and M. Nath, *J. Chem. Soc., Dalton Trans.*, 2003, **1**, 1–25.
23 D. T. Mitchell, S. B. Lee, L. Trofin, N. Li, T. K. Nevanen, H. Söderlund and C. R. Martin, *J. Am. Chem. Soc.*, 2002, **124**, 11864–11865.
24 R. A. Caruso, J. H. Schattka and A. Greiner, *Adv. Mater.*, 2001, **13**, 1577–1579.
25 P. Blanchard, P. Leriche, P. Frere and J. Roncali, in *Advanced functional polythiophene based on tailored precursors*, ed. T. A. Skotheim and J. R. Reynolds, CRC Press, Florida, 2007, pp. 1–77.
26 L. Zhai and R. D. McCullough, *J. Mater. Chem.*, 2004, **14**, 141–143.
27 O. Surucu, G. Bolat and S. Abaci, *J. Electroanal. Chem.*, 2013, **701**, 20–24.
28 H. Aebi, *Methods Enzymol.*, 1984, **105**, 121–126.
29 W. Chen, W. P. Cai, C. H. Liang and L. D. Zhang, *Mater. Res. Bull.*, 2001, **36**, 335–342.
30 T. Sakai, H. Enomoto, K. Torigoe, H. Sakai and M. Abe, *Colloids Surf., A*, 2009, **347**, 18–26.
31 K. S. Suslick and G. J. Price, *Annu. Rev. Mater. Sci.*, 1999, **29**, 295–326.

32 S. Eliyahu, A. Vaskevich and I. Rubinstein, *Thin Solid Films*, 2010, **518**, 1661–1666.
33 K. Kwon, K. Y. Lee, Y. W. Lee, M. Kim, J. Heo, S. J. Ahn and S. W. Han, *J. Phys. Chem. C*, 2006, **111**, 1161–1165.
34 K. C. Nguyen, *Adv. Nat. Sci.: Nanosci. Nanotechnol.*, 2012, **3**, 1–5.
35 A. J. Bard and L. R. Faulkner, *Electrochemical methods: fundamentals and applications*, Wiley, New York, 2nd edn, 2001.
36 N. Q. Jia, Z. Y. Wang, G. F. Yang, H. B. Shen and L. Z. Zhu, *Electrochem. Commun.*, 2007, **9**, 233–238.
37 L. Wang, J. Wang and F. Zhou, *Electroanalysis*, 2004, **16**, 627–632.
38 S. W. Ting, A. P. Periasamy, S. M. Chen and R. Saraswathi, *Int. J. Electrochem. Sci.*, 2011, **6**, 4438–4453.
39 A. W. Bott and W. R. Heineman, *Curr. Sep.*, 2004, **20**, 121–126.
40 S. Hashemnia, S. Khayatzadeh, A. A. Moosavi-Movahedi and H. Ghourchian, *Int. J. Electrochem. Sci.*, 2011, **6**, 581–595.
41 R. A. Kamin and G. S. Wilson, *Anal. Chem.*, 1980, **52**, 1198–1205.
42 M. Senel, E. Cevik and M. F. Abasiyanik, *Anal. Bioanal. Electrochem.*, 2011, **3**, 14–25.
43 P. Nien, T. Tung and K. Ho, *Electroanalysis*, 2006, **18**, 1408–1415.
44 P. Arun Prakash, U. Yogeswaran and S. M. Chen, *Talanta*, 2009, **78**, 1414–1421.
45 Z. Liu, B. Zhao, Y. Shi, C. Guo, H. Yang and Z. Li, *Talanta*, 2010, **81**, 1650–1654.
46 Q. Sheng, M. Wang and J. Zheng, *Sens. Actuators, B*, 2011, **160**, 1070–1077.
47 A. Liu, W. Dong, E. Liu, W. Tang, J. Zhu and J. Han, *J. Electrochim. Acta*, 2010, **55**, 1971–1977.